2020 IEEE/RSJ International Conference on Intelligent Robots and Systems (IROS)
October 25-29, 2020, Las Vegas, NV, USA (Virtual)

Simultaneous position-stiffness control of antagonistically driven twisted-coiled polymer actuators using model predictive control

Tuan Luong[1], Kihyeon Kim[1], Sungwon Seo[1], Jeongmin Jeon[1],
Ja Choon Koo[1], Hyouk Ryeol Choi[1] and Hyungpil Moon[1*]

Abstract— **Super-coiled polymer (SCP) artificial muscles have many interesting properties that show potentials for making high performance bionic devices. To realize human-like robotic devices from this type of actuator, it is important for the SCP driven mechanisms to achieve human-like performance, such as compliant behaviors through antagonistic mechanisms. This paper presents the simultaneous position-stiffness control of an antagonistic joint driven by hybrid twisted-coiled polymer actuation bundles made from Spandex and nylon fibers, which is a common human compliant behavior. Based on a linear model of the system, which is identified and verified experimentally, a controller based on model predictive control (MPC) is designed. The MPC performance is enhanced by the incorporation of time delay estimation to estimate model variations and external disturbances. The controlled system is verified through simulations and experiments. The results show the controller's ability to control the joint angle with the highest position error of 0.6 degrees while changing joint stiffness, verified with step command and sinusoidal reference with composite frequencies of 0.01Hz to 0.1Hz.**

I. INTRODUCTION

Nowadays, there is an increasing demand for development of human-like robotics applications, especially in rehabilitation or prosthesis fields. Although conventional actuators, such as electric motors, hydraulic actuators can obtain accurate position control, they also possess drawbacks, such as heavyweight, large volumes, high friction,.. Moreover, they are fundamentally different from biological organisms such as humans. Those disadvantages make them inappropriate for some specific applications. In the design of human like robotics application, it is desired to have light actuators with controllable stiffness, high power to weight ratio and human-like muscle properties.

Over the few decades, the development of artificial muscles resulted in new actuators, such as electroactive polymers [1], pneumatic actuators [2], shape memory alloy actuators [3], super-coiled polymer (SCP) actuators [4], [5], [6], [7], [8]. In terms of low cost, large stroke, high work density and high load carrying capabilities, the SCP actuator is emerging as a potential actuator. Due to its interesting properties, extensive research has been conducted on SCP actuators. Many variations of SCP actuators have been made since its introduction [9], [10]. Both phenomenal models and physics-based models have been proposed to capture the relationship between temperature, force, and displacement of the actuator [5], [11], [12], [13], [14]. Various position controllers and force controllers have been developed for this type of actuator. However, there is still a lack of realization of SCP actuators to human-like robotic implementations. Especially, design and control of SCP actuator driven mechanisms that have human-like compliant behaviors is still an open research problem.

It was known that compliance is critical to stabilize our arm motion and to achieve safe working performance. Humans achieve compliant joint actuation by co-contracting antagonistic muscles. The ability to co-contract these antagonistic compliant muscles allows independent control over both joint stiffness and joint position. In our previous work[15], a torque-based impedance control for antagonistically driven SCP actuators has been proposed enabling joint angle control with variable impedance. This paper presents another control method, in which both position and stiffness of an SCP actuator driven antagonistic robot joint is realized by model predictive control.

In this work, bundles of SCP actuators are used to realize a compliant antagonistic joint. The bundle properties are characterized to obtain the relationship between temperature, force, length. The relationship between the actuator's stiffness with its actuator's temperature is discussed. In addition, a linear model of the SCP bundle is also developed. The model parameters are determined through experiments. The verified model, which is in the form of the state-space equations is used to design the controller.

Model predictive control (MPC) is utilized in our control approach. Based on the system's model, MPC is able to predict the system behavior across a discrete finite time horizon to produce optimal or sub-optimal control actions for a cost function given specific constraints. Therefore, MPC allows the actuators to achieve its best performance at its limits, but still safe in its working range. Considering the actuator's highly nonlinear properties, the time delay estimation (TDE) is designed to compensate for the unmodeled dynamics and external disturbances, which helps increase the robustness of the controller. The effectiveness of the control design is verified through simulations and experiments.

The remaining of this paper is organized as follows. In Section II actuation bundle properties are studied and

*This research was supported by the convergence technology development program for bionic arm through the National Research Foundation of Korea (NRF) funded by the Ministry of Science, ICT and Future Planning (No. 2014M3C1B2048175).

[1] Ja Choon Ko, Hyouk Ryeol Choi and Hyungpil Moon are with Faculty of Mechanical Engineering, Sungkyunkwan University, 2066, Seobu-ro, Jangan-gu, Suwon, South Korea (hyungpil@skku.edu)

The other authors are students at Faculty of Mechanical Engineering, Sungkyunkwan University, 2066, Seobu-ro, Jangan-gu, Suwon, South Korea.

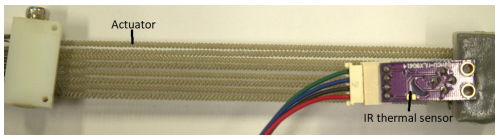

Fig. 1. A Spandex-nylon SCP bundle fabricated in-house with a IR thermal sensor

a model for the Spandex-nylon SCP actuator is presented in Section III. Our control design method is discussed in Section IV. Simulation results and experimental results are presented in Section V. We conclude the paper in Section VI.

II. ACTUATOR PROPERTY CHARACTERIZATION

In this work, to increase the force capability of the system, bundle configuration of super-coiled polymer actuators is used in the antagonistic mechanism. In this section, we briefly introduce the Spandex and nylon fibers bundle and experimental setups for actuator characterization.

A. Test bed setup for characterization of Spandex and nylon SCP bundles

The materials of the actuator are Spandex yarn (Creora®, Hyosung Inc.) and nylon conductive sewing thread (Shield-exTM No. 200121235343B). A bundle consists of 8 single Spandex-nylon SCP actuators, which was previously introduced in [16]. In which, four fibers were fabricated with the counter-clockwise rotation of the motor, and the other four were fabricated with clockwise rotation. The configuration is set to keep the torque balance of the bundle. The bundle's length is equal to the length of each actuator (105 mm at the ambient temperature). A fabricated nylon and Spandex-nylon bundle is shown in Fig.1.

To characterize the SCP actuator, testbeds developed in [16] are used as shown in Fig. 2a and Fig 2b. Isothermal and isometric tests are carried out using the experimental setup in Fig. 2a, where the actuator connected between the testbed and a load cell (CB1A, 2kgf, DACEL CO.). The length of the actuator is accurately controlled by a stepper motor (ZCV620-C-N) and a motor controller (DS102, SURUGA SEIKI CO.) with the resolution of $1\mu m$. Actuators are applied power through electrical leads which are connected to a power supply. The actuator's temperature was measured with an IR thermal sensor. The temperature and the force values are recorded using NI cDAQ 9174 and Labview.

For the dynamic test, the experimental setup shown in Fig 2b was used. In which, the actuator is connected between a load and a load cell (CM, 50kgf, DACEL CO.). The load is attached to a magnetic sensor (MLI-T80, OPKON), which can be used to measure the load's position. The temperature was measured with the same IR thermal sensor.

B. Actuator properties

The same isothermal and isometric testing processes to [16] have been conducted to measure the properties of the fabricated SCP actuators. In the isothermal test, strains between 0% and 30% are exerted to the actuator

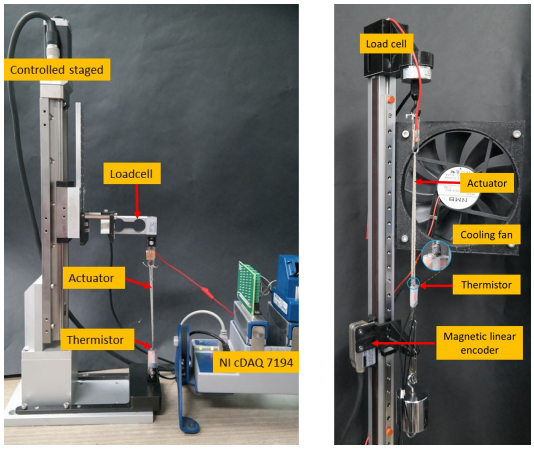

(a) Isometric and isothermal test setup (b) Dynamic test setup

Fig. 2. Experimental setup for property characterization of the SCP bundle

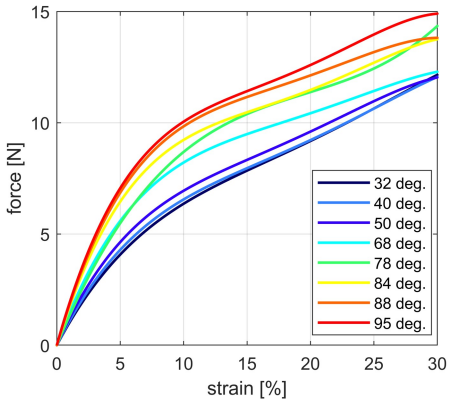

Fig. 3. A force-strain profile of Spandex-nylon SCP actuators at various temperature conducted at 0.2mm/s elongation rate

with the controlled stage at different deformation rates of $0.2mm/s, 0.4mm/s, 1mm/s$. The temperature of the actuator has a variation of $\pm 2^{\circ}C$ during the isothermal test; however, it is considered isothermal. Based on the isothermal test, third order polynomial fitting has been done to find the relationship between strain and force at different temperatures. The results at an elongation rate of $0.2mm/s$ in Fig. 3 shows that at the same strain, the force value is higher when the temperature increases. This implies that at the same strain, the actuator's stiffness increases when the temperature increases. The results obtained at other elongation rates shows the same temperature stiffness relationship of the SCP bundle. Fig. 4 shows the results of the force-strain curves obtained at each temperature with different elongation rates.

The isometric test shows the same linear relationship between the actuator's temperature and force at fixed strain as results obtained in [16].

III. ACTUATOR MODELING

This section presents the actuator's model, which includes a thermo-electrical model showing the relationship between

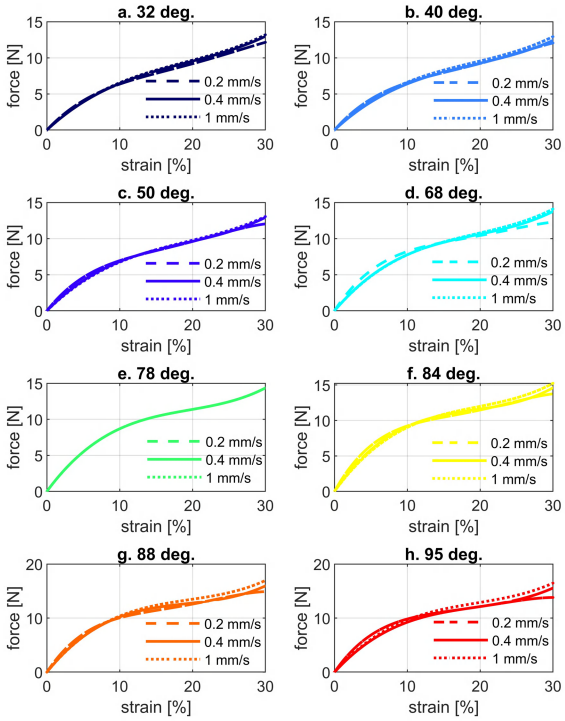

Fig. 4. A force-strain profile of Spandex-nylon SCP actuators at various temperature conducted at various elongation rate

the actuation bundle's temperature and applied power, and a thermo-mechanical model showing the relationship between temperature-force-strain of the bundle.

A. Thermo-electrical model

Similar to a single SCP actuator, the thermo-electrical model of a SCP bundle can be described by the following Joule heating model:

$$C_{th}\frac{dT(t)}{dt} = P(t) - \lambda(T - T_{amb}) \tag{1}$$

where C_{th} is the thermal mass of the actuator, $P(t) = \frac{V^2}{R}$ is the Joule heating that is applied to the bundle, and λ is the absolute thermal conductivity of the bundle in its ambient environment. The same method here is also used to find C_{th} and λ through experimental data. To increase the cooling speed, electric fans are used. The parameters obtained from the experimental data are shown in Table I.

B. Thermo-mechanical model

A linear model of the Spandex-nylon SCP bundle is used for the MPC control design. The unmodel-dynamics and external disturbances are estimated by our time delay estimation term in the control design.

$$F = b\dot{x} + kx + c(T - T_{amb}) \tag{2}$$

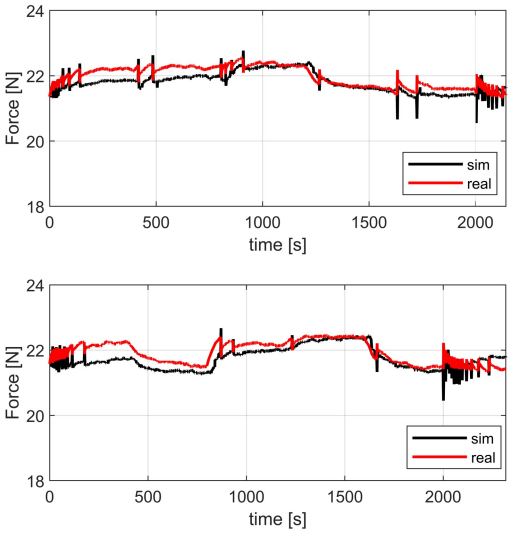

Fig. 5. Modeling results of the Spandex-nylon actuator lifting 1.9kg load

where b, k and c are the damping, spring stiffness of the actuator, and temperature effect on the actuator force, respectively. The value of c is identified based on the experimental data showing temperature effect on the actuator's force. After c is identified, k can be found based on data from isothermal experiments, where constant elongation rates are used. The parameters for thermo-mechanical model are shown in Table I.

To verify the model, different step voltage levels are applied to the actuator in the experimental setup in Fig. 2b. A load of 1.9kg was used. Modeling results can be seen in Fig. 5.

TABLE I
SPANDEX-NYLON SCP SYSTEM PARAMETERS

Parameter	Value
Actuator's mass m	22 (g)
Resistance R	3.4 (Ω)
Thermal mass C_{th}	7.81 $(J/^\circ C)$
Heat conductivity λ	0.03 ($W/^\circ C$)
damping coefficient b	176.49 ($N/m.s$)
spring coefficient k	319 (N/m)
temperature coefficient c	0.03 ($N/^\circ C$)
pulley radius r	0.025 (mm)

C. Antagonistic joint model

The equation of motion of antagonistic joint is given as follows.

$$J\ddot{\theta} = (F_2 - F_1)r \tag{3}$$

where J is the inertia moment of the antagonistic joint, θ is the joint angle, F_i is the force applied by actuator i $(i = 1, 2)$ and r is the pulley radius.

From the thermo-electrical model (1), thermo-mechanical model (2) of the bundle and the antagonistic joint model (3), one can easily have the state equation of the system in the form of Eq. 4

$$\dot{\boldsymbol{x}} = \boldsymbol{A}_c\boldsymbol{x} + \boldsymbol{B}_c\boldsymbol{u} \tag{4}$$

where $\boldsymbol{x} = [\theta, \dot{\theta}, T_1, T_2]^T$, $\boldsymbol{u} = [u_1, u_2]^T$, $\boldsymbol{A}_c, \boldsymbol{B}_c$ are constant matrices, T_i is the temperature of the actuator i $(i = 1, 2)$.

IV. MODEL PREDICTIVE CONTROL

MPC is an advanced control technique that uses online optimization performed over a prediction horizon to calculate the best control actions. One of the advantages of MPC is the integration of the system model and constraints into a single controller. Although the optimization is run over the prediction horizon, only the first control action is taken. The optimization is then re-calculated after receiving feedback from the current system in the next time step.

Following, we introduce the linear discrete-time model of the antagonistic driven SCP actuators and the constrained cost function optimization problem.

A. Discrete linear model of the antagonistically driven SCP actuators

From the modeling results obtained in the section III-C, if we consider the system's disturbance, the model of the antagonistic joint driven by SCP actuators can be expressed as

$$\dot{\boldsymbol{x}} = \boldsymbol{A}\boldsymbol{x} + \boldsymbol{B}\boldsymbol{u} + \boldsymbol{d} \tag{5}$$

where $\boldsymbol{d}$ is the disturbance vector. One can convert the continuous-time system to an equivalent discrete-time system using a standard discretization procedure yielding

$$\boldsymbol{x}_{k+1} = \boldsymbol{A}_d\boldsymbol{x}_k + \boldsymbol{B}_d\boldsymbol{u}_k + \boldsymbol{d}_k \tag{6}$$

where

$$\boldsymbol{A}_d = e^{\boldsymbol{A}T}$$
$$\boldsymbol{B}_d = \int_0^T e^{\boldsymbol{A}T}\boldsymbol{B}d\tau$$
$$d_k = \int_0^T e^{\boldsymbol{A}T}d(kT + T - \tau)\boldsymbol{d}\tau$$

The MPC problem can be formulated as

$$\min_{\boldsymbol{u}} \sum_{k=i}^{i+N_p-1} \xi(\theta_k^d - \theta_k)^2 + \mu\boldsymbol{u}_k^T\boldsymbol{u}_k + \gamma(T_{1k} + T_{2k} - K|\theta_k^d| - T_{sk})^2 \tag{7}$$

subjected to:

$$\begin{aligned}\boldsymbol{x}_{k+1} &= \boldsymbol{A}_k\boldsymbol{x}_k + \boldsymbol{B}_k\boldsymbol{u}_k + \boldsymbol{d}_k, k = i, .., i + N_p - 1\\ \boldsymbol{u}_{min} &\le \boldsymbol{u}_k \le \boldsymbol{u}_{max}, k = i, .., i + N_p - 1\end{aligned} \tag{8}$$

where N_p is the prediction horizon, ξ, μ, γ are scalar weights which penalize input deviations, state deviation, and total temperature deviation, respectively. The target temperature sum of two actuation bundles relates the desired joint angle through a constant K and includes an offset value of T_{sk}, which is also related to the joint's stiffness. $\boldsymbol{u}_{min} \in \mathbb{R}^2, \boldsymbol{u}_{max} \in \mathbb{R}^2$. The optimization problem returns $\boldsymbol{u} = [\boldsymbol{u}_i, \boldsymbol{u}_{i+1}, \ldots, \boldsymbol{u}_{i+N_p-1}]^T$

The optimization is solved using code generated by CVXGEN [17], a web-based tool for generating convex optimization solvers. The code is then converted to .dll file to be used in Labview for experiments. The solver can run up to 300Hz.

B. Constraint definition and time delay estimation

It is observed that below the power limit level, some high power levels still break the actuator due to overheating at steady state. Therefore, instead of using constant power limits for the MPC, we calculate current power limits of the actuator based on the actuator's maximum working temperature, its current temperature, and heat transfer model.

From the continuous-time heat transfer model in section III-A, a discrete-time model can be expressed as

$$C_{th}\frac{T_{k+1} - T_k}{T} = P_k - \lambda(T_k - T_{amb}) \tag{9}$$

From 9, the power constraint can be set as follows

$$\begin{aligned}P_{kmin} &= C_{th}\frac{T_{min} - T_k}{T} + \lambda(T_k - T_{amb})\\ P_{kmax} &= C_{th}\frac{T_{max} - T_k}{T} + \lambda(T_k - T_{amb})\end{aligned} \tag{10}$$

In this work, the disturbance vector $\boldsymbol{d}$ is estimated by

$$\hat{\boldsymbol{d}}_{k+i-1} = \boldsymbol{d}_{k-1}, i = 1 \ldots N_p \tag{11}$$

where $\boldsymbol{d}_{k-1} = \boldsymbol{x}_k - \boldsymbol{A}_d\boldsymbol{x}_{k-1} - \boldsymbol{B}_d\boldsymbol{u}_{k-1}$. It can be shown in that the error between the actual and estimated values of $\boldsymbol{d}_{k+i-1}$ is $\alpha + \mathcal{O}(T)$, where α is a positive number.

V. CONTROL IMPLEMENTATION

To verify the control design, some simulations and experiments have been carried out. Simulation is carried out in MATLAB, and experiments are done through LabView environment. The prediction horizon is chosen as $N_p = 20$.

A. Simulation results

As the traditional MPC is known to require a relatively accurate model to provide predictive performance, the time delay estimation is added to ease this model dependency. The effectiveness of the time delay estimation to MPC performance is shown through set-point regulation simulation in Figs. (7). To verify the robustness of the system with external disturbances, the disturbance $\boldsymbol{d}_k = (0.0005(1 + 0.01\sin(2\pi 0.01t)))[1, 1, 1, 1]^T$ is assumed in the simulation. It can be seen that the MPC with TDE has better performance in terms of small position errors, which shows the effectiveness of the designed controller in maintaining the robust working performance of the system.

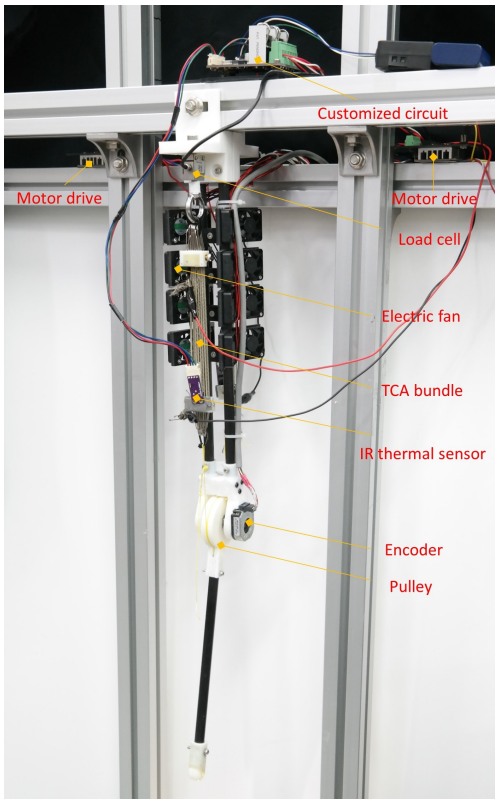

Fig. 6. One DoF antagonistic joint driven by SCP bundle actuators

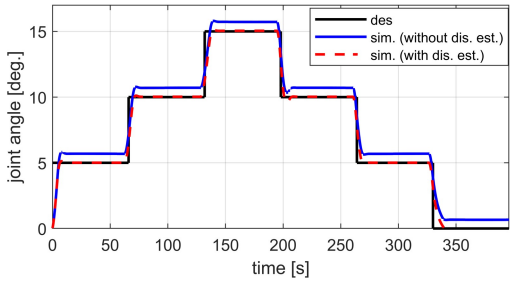

Fig. 7. Simulation results of MPC control with and without time delay estimation

B. Experimental results

The experimental control tests have been carried out using the experimental setup shown in Fig. 6. A general power supply (30V, 5A) and a motor driver module were used to supply power to actuators. The motor driver is controlled by PWM signals sent from NI cDAQ 9174. Joint encoder is measured using (ATM203-512). The sampling frequency is 25Hz. The controller parameters were chosen as: $\xi = 10^-4, \mu = 5000, \gamma = 10, K = 200, Ts$ varies from $5°C$ to $15°C$. In the experiment, a weight of 10g was added to the end of the arm as a disturbance source. The maximum temperature of each actuator is set as $80°C$.

The first experiment tests the ability of the controller to hold the joint at a constant angle while changing the joint stiffness. In this experiment, a joint angle of 5 degrees and various step total temperature values, which are related to

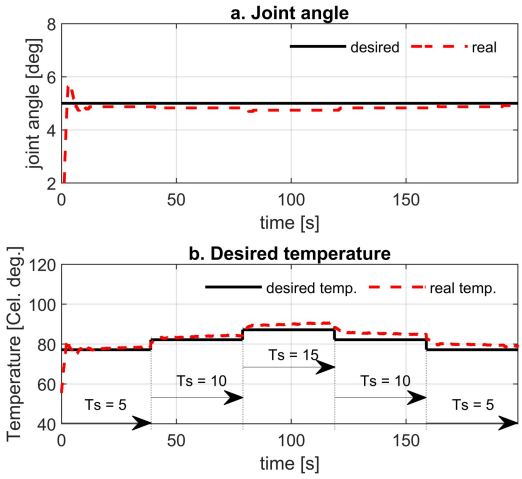

Fig. 8. Experimental results for keeping a constant joint angle while varying a multi-step total temperature, which is related to stiffness

stiffness, are desired. It can be seen from Fig. 8 that, once the desired angle is reached, the angle error remains less than 0.3 degrees while varying the total temperature(corresponding to the target temperature offset from $5°C$ to $15°C$). The result implies the possibility of adjusting joint stiffness while maintaining a relatively constant joint angle.

Fig. 9 shows the total temperature and joint angle while the joint angle is stepped between 5 degrees and 10 degrees, and the target temperature offset T_s is stepped between $5°C$ and $10°C$. It can be seen that, while the resultant temperature varies in step around 30%, the desired step joint angle can be followed. The joint angle error at the steady-state remains less than 0.5 degrees.

Fig. 10 shows the results when the joint angle is desired to track a sinusoidal waveform (with composite frequencies of 0.02Hz and 0.1Hz), and the temperature offset is commanded to follow a sinusoidal wave with a frequency of 0.01Hz, which results in a sinusoidal waveform with composite frequencies of 0.01Hz, 0.02Hz, and 0.1Hz for the required total temperature. Although the total temperature is changed largely, the steady-state tracking error is maintained less than 0.6 degrees, which shows the controller's effectiveness.

The results, shown in Fig. 9 and Fig. 10, therefore, verify the controller's ability to adjust joint stiffness while the desired angle also varies. This result is due to the higher weight in the joint angle tracking term in the MPC cost function.

C. Discussions

From simulation and experimental results, it can be seen that the proposed control frame is suitable for simultaneous position-stiffness control of the antagonistic system driven by Spandex-nylon bundles. At its heart, the model predictive control plays an important role in providing model-based predictive behaviors, which give the best control actions over the prediction horizon and take into account the physical constraints of the actuators. The time delay estimation

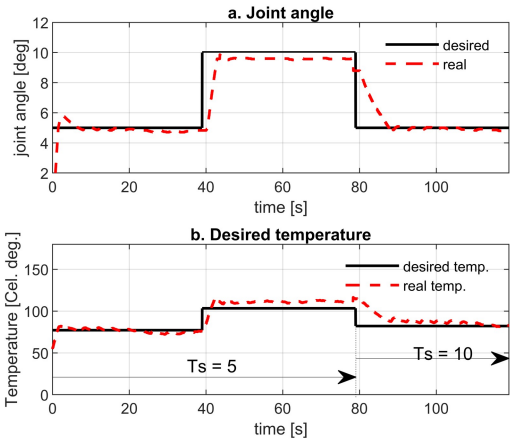

Fig. 9. Experimental results for controlling a multi-step joint angle and a multi-step total temperature sum simultaneously

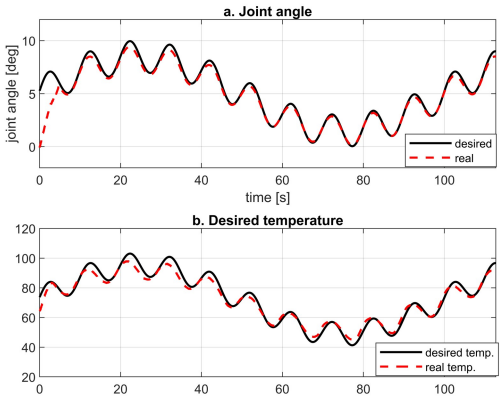

Fig. 10. Experimental results of controlling a sinusoidal angle (with composite frequencies of 0.02hz and 0.1hz) and a sinusoidal temperature (0.01hz) simultaneously

also contributes to the controller's performance by helping compensate the actuator's nonlinear properties and external disturbances.

The performance of the proposed controller can be improved by using real-time systems that can provide fast system feedback for mpc and reduce time delay estimation errors.

VI. CONCLUSIONS

This paper presents properties characterization, modeling of Spandex-nylon bundles, and MPC based position-stiffness control of antagonistic joint driven by the Spandex-nylon bundle. The work shows the possibility to obtain a joint position target and simultaneously alter the stiffness of the joint.

From this work, it can be extended to implement multi-DOF Spandex-nylon bundle driven devices with controllable stiffness for safe interaction with humans.

APPENDIX

The disturbance error term $\boldsymbol{d}_{k,i} = \boldsymbol{d}_{k+i-1} - \boldsymbol{d}_{k-1}$ can be separated in to model uncertainties and external disturbances, which can be represented as

$$\boldsymbol{d}_{k,i} = \boldsymbol{h}(\boldsymbol{x}) + \boldsymbol{d}_{ext} \tag{12}$$

Since it is well-known that many hysteresis operators are Lipschitz continuous [18], considering the hysteresis properties of the SCP actuator as shown in [12], it can be assumed that $\boldsymbol{h}(\boldsymbol{x})$ is Lipschitz continuous. From the Lipschitz continuous condition, one obtains $\boldsymbol{h}(\boldsymbol{x}) = \mathcal{O}(T)$.

The external disturbance term $\boldsymbol{d}_{ext}$ can also be separated into continuous and discontinuous terms.

$$\boldsymbol{d}_{ext} = \boldsymbol{d}_{cont} + \boldsymbol{d}_{disc} \tag{13}$$

It is assumed here that $\boldsymbol{d}_{disc}$ is bounded by $\boldsymbol{d}_{disc} \leq \alpha$, where γ is a positive value. if $\boldsymbol{d}_{cont}(t)$ and its time derivative is bounded, $\boldsymbol{d}_{disc} = \mathcal{O}(T^2)$ [19]. In summary, the time delay estimation error is $\alpha + \mathcal{O}(T)$

REFERENCES

[1] Y. Bar-Cohen, V. Cardoso, C. Ribeiro, and S. Lanceros-Méndez, "Electroactive polymers as actuators," in *Advanced piezoelectric materials*, pp. 319–352, Elsevier, 2017.

[2] R. M. Robinson, C. S. Kothera, R. M. Sanner, and N. M. Wereley, "Nonlinear control of robotic manipulators driven by pneumatic artificial muscles," *IEEE/ASME Transactions on Mechatronics*, vol. 21, no. 1, pp. 55–68, 2016.

[3] D. Grant and V. Hayward, "Variable structure control of shape memory alloy actuators," *Control Systems, IEEE*, vol. 17, no. 3, pp. 80–88, 1997.

[4] C. S. Haines, M. D. Lima, N. Li, G. M. Spinks, J. Foroughi, J. D. Madden, S. H. Kim, S. Fang, M. J. de Andrade, F. Göktepe, *et al.*, "Artificial muscles from fishing line and sewing thread," *science*, vol. 343, no. 6173, pp. 868–872, 2014.

[5] M. C. Yip and G. Niemeyer, "High-performance robotic muscles from conductive nylon sewing thread," in *Robotics and Automation (ICRA), 2015 IEEE International Conference on*, pp. 2313–2318, IEEE, 2015.

[6] S. M. Mirvakili, A. R. Ravandi, I. W. Hunter, C. S. Haines, N. Li, J. Foroughi, S. Naficy, G. M. Spinks, R. H. Baughman, and J. D. Madden, "Simple and strong: Twisted silver painted nylon artificial muscle actuated by joule heating," in *SPIE Smart Structures and Materials+ Nondestructive Evaluation and Health Monitoring*, pp. 90560I–90560I, International Society for Optics and Photonics, 2014.

[7] S. Kianzad, M. Pandit, A. Bahi, A. R. Ravandi, F. Ko, G. M. Spinks, and J. D. Madden, "Nylon coil actuator operating temperature range and stiffness," in *SPIE Smart Structures and Materials+ Nondestructive Evaluation and Health Monitoring*, pp. 94301X–94301X, International Society for Optics and Photonics, 2015.

[8] T. A. Luong, S. Seo, J. C. Koo, H. R. Choi, and H. Moon, "Differential hysteresis modeling with adaptive parameter estimation of a supercoiled polymer actuator," in *2017 14th International Conference on Ubiquitous Robots and Ambient Intelligence (URAI)*, pp. 607–612, 2017.

[9] C. Xiang, H. Yang, Z. Sun, B. Xue, L. Hao, M. A. Rahoman, and S. Davis, "The design, hysteresis modeling and control of a novel sma-fishing-line actuator," *Smart Materials and Structures*, vol. 26, no. 3, p. 037004, 2017.

[10] S. Y. Yang, K. H. Cho, Y. Kim, M.-G. Song, H. S. Jung, J. W. Yoo, H. Moon, J. C. Koo, H. R. Choi, *et al.*, "High performance twisted and coiled soft actuator with spandex fiber for artificial muscles," *Smart Materials and Structures*, vol. 26, no. 10, p. 105025, 2017.

[11] A. Abbas and J. Zhao, "A physics based model for twisted and coiled actuator," in *Robotics and Automation (ICRA), 2017 IEEE International Conference on*, pp. 6121–6126, IEEE, 2017.

[12] T. A. Luong, K. H. Cho, M. G. Song, J. C. Koo, H. R. Choi, and H. Moon, "Nonlinear tracking control of a conductive supercoiled polymer actuator," *Soft robotics*, 2017.

[13] T. Arakawa, K. Takagi, K. Tahara, and K. Asaka, "Position control of fishing line artificial muscles (coiled polymer actuators) from nylon thread," in *SPIE Smart Structures and Materials+ Nondestructive Evaluation and Health Monitoring*, pp. 97982W–97982W, International Society for Optics and Photonics, 2016.

[14] L. Sutton, H. Moein, A. Rafiee, J. D. Madden, and C. Menon, "Design of an assistive wrist orthosis using conductive nylon actuators," in *Biomedical Robotics and Biomechatronics (BioRob), 2016 6th IEEE International Conference on*, pp. 1074–1079, IEEE, 2016.

[15] T. Luong, K. Kim, S. Seo, J. H. Park, Y. Kim, S. Y. Yang, K. H. Cho, J. C. Koo, H. R. Choi, and H. Moon, "Impedance control of a high performance twisted-coiled polymer actuator," in *2018 IEEE/RSJ International Conference on Intelligent Robots and Systems (IROS)*, pp. 8701–8706, IEEE, 2018.

[16] T. Luong, K. Kim, S. Seo, J. H. Park, Y. Kim, S. Y. Yang, K. H. Cho, J. C. Koo, H. R. Choi, and H. Moon, "Modeling and position control of a high performance twisted-coiled polymer actuator," in *2018 15th International Conference on Ubiquitous Robots (UR)*, pp. 73–79, IEEE, 2018.

[17] J. Mattingley and S. Boyd, "Cvxgen: A code generator for embedded convex optimization," *Optimization and Engineering*, vol. 13, no. 1, pp. 1–27, 2012.

[18] H. Logemann, E. P. Ryan, and I. Shvartsman, "A class of differential-delay systems with hysteresis: asymptotic behaviour of solutions," *Nonlinear Analysis: Theory, Methods & Applications*, vol. 69, no. 1, pp. 363–391, 2008.

[19] W.-C. Su, S. V. Drakunov, and U. Ozguner, "An o (t/sup 2/) boundary layer in sliding mode for sampled-data systems," *IEEE Transactions on Automatic Control*, vol. 45, no. 3, pp. 482–485, 2000.